JOURNAL OF GEOPHYSICAL RESEARCH, VOL. 107, NO. D24, 4790, doi:10.1029/2002JD002190, 2002

On the evolution of pollution from South and Southeast Asia during the winter-spring monsoon

Mahesh J. Phadnis[1]

Science Technology and Environmental Policy, Woodrow Wilson School of Public and International Affairs, Princeton University, Princeton, New Jersey, USA

Hiram Levy II and Walter J. Moxim

Geophysical Fluid Dynamics Laboratory, NOAA, Princeton, New Jersey, USA

Received 8 February 2002; revised 2 May 2002; accepted 13 June 2002; published 26 December 2002.

[1] The NOAA Geophysical Fluid Dynamics Laboratory three-dimensional Global Chemical Transport Model (GFDL GCTM) is used to examine the winter-spring evolution of pollution (fossil fuel combustion and biomass burning) from South and Southeast Asia with special focus on the Indian Ocean region. We find that during the monsoonal winter-spring outflow, pollution over the Indian Ocean north of the ITCZ is concentrated in the maritime boundary layer and originates from both regions. South Asian emissions dominate over the Arabian Sea and the Western Indian Ocean, while the Southeast Asian emissions have the greatest impact over the Bay of Bengal and Eastern Indian Ocean. Over these oceanic regions, CO pollution in both source regions, most of which is from biomass burning, accounts for 30–50% of the boundary layer CO. It is transported equatorward from South and Southeast Asian source regions and episodically lofted into the upper troposphere by tropical convection events. This transport path has a noticable impact (10–20%) on total CO at 300 mb and produces a maximum in a tropical belt over and north of the ITCZ. Another free troposphere transport path, primarily open to Southeast Asian emissions, carries CO from that region out over the North Pacific and around the Northern Hemisphere. O_3 production is driven by NO_x, which, unlike CO, comes almost equally from biomass burning and fossil fuel combustion in this region and has a chemical lifetime of a few days or less. The resulting NO_x distributions, while qualitatively similar to CO, have much steeper gradients, are transported much less widely, have a much lower background, and over the Indian and Pacific Oceans, are strongly dominated by pollution. O_3 resulting from these anthropogenic sources generally exhibits patterns similar to those found for CO and NO_x. Pollution accounts for 20–50% of the near-surface O_3 and 5–10% of the O_3 in the upper troposphere. South and Southeast Asian emissions only produce 25% of the boundary layer O_3 in the continental source regions. The maximum impact of the emissions occurs over the Indian Ocean (25–40%) with comparable contributions from O_3 produced in the continental emission regions and O_3 produced over the ocean by transported precursors. Convective lifting of the transported pollution O_3 supplies ~10% of the O_3 in the tropical upper troposphere. While both emission regions have modest impacts on O_3 (5–10%) outside of the Indian Ocean region, Southeast Asian pollution impacts free troposphere O_3 in a midlatitude belt across the North Pacific, similar to NO_x. *INDEX TERMS:* 0345 Atmospheric Composition and Structure: Pollution—urban and regional (0305); 0365 Atmospheric Composition and Structure: Troposphere—composition and chemistry; 0368 Atmospheric Composition and Structure: Troposphere—constituent transport and chemistry; *KEYWORDS:* South and Southeast Asia, pollution outflow, winter spring monsoon, Asian pollution, INDOEX, ITCZ

Citation: Phadnis, M. J., H. Levy II, and W. J. Moxim, On the evolution of pollution from South and Southeast Asia during the winter-spring monsoon, *J. Geophys. Res.*, *107*(D24), 4790, doi:10.1029/2002JD002190, 2002.

1. Introduction

[2] The increasing levels of greenhouse gases, as well as radiatively active aerosols, in the Earth's climate system are observed to be a direct consequence of human activities.

[1]Now at Earth Tech, Inc., Concord, Massachusetts, USA.

0148-0227/02/2002JD002190$09.00

These activities also lead to anthropogenic emissions of NO_x, CO, and VOCs, which generate tropospheric O_3, a greenhouse gas and a key secondary pollutant playing a very important role in the formation of OH, the primary atmospheric oxidant [e.g., *Intergovernmental Panel on Climate Change (IPCC)*, 2001].

[3] Anthropogenic NO_x emissions from Asia, which are currently dominated by fossil fuel combustion [e.g., *van Aardenne et al.*, 1999], domestic biofuel use [*Streets and Waldhoff*, 1998], and seasonal open-field biomass burning [*Galanter et al.*, 2000], are of particular concern because of rapid economic development and population growth in the region (http://www.worldbank.org/data). It is expected that future NO_x emissions from Asia will exceed those from Europe and North America combined. For example, *van Aardenne et al.* [1999] estimate that Asian NO_x emissions from fossil fuel combustion will increase from ~6 TgN/yr in 1990 to >25 TgN/yr in 2020 under a no-further-control scenario, although revised estimates indicate a values <20 TgN/yr (D. G. Streets, personal communications). In comparison the worldwide amount in the mid-1980s through early 1990s was ~25 TgN/yr [e.g., *Benkovitz et al.*, 1996; *Olivier et al.*, 1996]. O_3 concentrations in the lower troposphere have already increased significantly in India [*Naja and Lal*, 1996], and the impact of South and Southeast Asian pollution on the pristine Indian Ocean is currently a very active area of research [*Lelieveld et al.*, 2001].

[4] The meteorology over South Asia is dominated by the existence of two major flow regimes characterized by a complete reversal of low level winds driven by a land-ocean heat gradient. These winter (summer) monsoons are caused by high (low) pressure over land leading to clear sky (cloudy) conditions and persistent northeasterly (southwesterly) airflows. Particularly, during the winter monsoon (between December and March), flows emanating from the landmass of Asia are very shallow north-northeasterlies that turn rapidly with altitude and have a strong westerly component above the boundary layer (~2 km) [e.g., *Krishnamurti et al.*, 1997a]. This wintertime flow from South Asia is responsible for the cross-equatorial transport between the polluted north and the pristine south affected by eddies at the ITCZ [*Krishnamurti et al.*, 1998]. *Krishnamurti et al.* [1998] have also shown that high concentrations of aerosols over the ocean are a result of three meteorological factors: strong surface northerly wind flow; a shallow boundary layer (400–800 m thick); and general subsidence which suppresses rainfall over South Asia thus minimizing wet removal. Further, *Krishnamurti et al.* [1997b] carrying out passive tracer studies during the winter monsoon identified three major regions of inflow to the ITCZ: Arabian sea, Bay of Bengal and Southeastern Indian Ocean. This equatorward monsoonal flow over the North Indian Ocean into the convectively active ITCZ provides an efficient mechanism for transporting surface pollution from South Asia into the tropical upper troposphere/lower stratosphere where, because of stronger winds and longer lifetimes, rapid long-range transport can occur.

[5] Although there exist sporadic measurements of trace chemical species over South Asia, until recently there were few chemical measurements over the Indian Ocean. Surface ozone measurements carried out on the Soviet American Gases and Aerosols (SAGA) cruise during May–June 1987 in the eastern Indian Ocean found ~10 ppbv near the equator increasing rapidly to ~30 ppbv at 30°N [*Johnson et al.*, 1990]. Recent ship measurements during spring 1996 indicated sharp increases in CO, CO_2 and aerosol surface concentrations from the southern to the northern Indian Ocean approaching South Asia [*Rhoads et al.*, 1997]. CO increased from background levels of ~50 ppbv in the southern hemisphere to >120 ppbv north of the equator, aerosol concentrations increased by a factor of 4, and surface ozone exhibited a latitudinal gradient with a minimum (~6 ppbv) near the equator. In another study, *Lal et al.* [1998] reported similar findings with CO as high as 200 ppbv near coastal India and O_3 levels increased from <10 ppbv at the equator to ~100 ppbv near the coast. Furthermore, their ozone levels correlated well with aerosol mass data indicating a common source and transport pathway.

[6] Recently, extensive measurements from a variety of platforms were carried out as a part of the Indian Ocean Experiment (INDOEX) with understanding the radiative forcing of atmospheric aerosols on a regional and global scale as its primary objective [*Ramanathan et al.*, 1996]. Along with aerosols, CO and O_3 were also measured. The field campaign provided startling evidence of the presence of substantial amounts of particulate matter and gaseous pollution in the air masses arriving over the Indian Ocean from South Asia. In addition, a thick extensive haze layer was also persistently observed over the Northern Indian Ocean with clear skies south of the ITCZ [*Lelieveld et al.*, 2001]. Surface level measurements of CO and O_3 during the Intensive Field Phase (IFP-99) of INDOEX exhibited a decreasing concentration of both species from the northern to the southern Indian Ocean. Ozone mixing ratios ranged from 50–70 ppbv near the Indian coast to as low as 5 ppbv south of the ITCZ. Similarly, CO levels ranged from ~300 ppbv in the north to ~50 ppbv in the south. Meteorological analysis during the IFP-99 indicated the presence of four preferred lower tropospheric paths of airflow in the Indian Ocean region. They were labeled the "Southeast Asia plume", "Indo-Gangetic plume", "Bombay plume" and "Arabia plume" [*Lelieveld et al.*, 2001].

[7] In this paper, we use the GFDL GCTM to examine the various transport pathways and associated pollution sources that influence the trace gas composition over the Indian Ocean during the northern hemisphere winter-spring monsoon season (January, February and March - JFM), the same season as the INDOEX campaign. We focus on quantifying the contributions of anthropogenic emissions from South and Southeast Asia to the observed levels of NO_x, CO and O_3 over the Indian Ocean and, in the case of Southeast Asia, also over the North Pacific.

2. Global Chemical Transport Model (GCTM)

[8] The NOAA Geophysical Fluid Dynamics Laboratory Global Chemical Transport Model (GFDL GCTM) is employed, in separate integrations, to simulate global fields of carbon monoxide (CO), nitrogen oxides (NO_x), and ozone (O_3). The GCTM has a horizontal resolution of ~265 km × 265 km and 11 sigma (terrain following) levels from the surface to 10 mbar [see *Mahlman and Moxim*, 1978; *Levy et al.*, 1982, 1985; *Levy and Moxim*, 1989]. The model is driven by 12 months of 6-hour time-averaged

wind, temperature, and precipitation fields from a general circulation model (see *Manabe et al.* [1974] and *Manabe and Holloway* [1975] for details of the parent GCM). Although neither the parent GCM nor the GCTM contain diurnal insolation or interannual variability, the self-consistent three-dimensional wind, temperature, and precipitation fields realistically simulate large-scale regional and global transport [*Moxim*, 1990; *Moxim et al.*, 1996]. While able to simulate large-scale synoptic features of weather, finer subgrid-scale processes are represented by diffusion-based parameterizations for horizontal subgrid-scale transport, vertical subgrid-scale transport due to moist and dry convection, and shear-dependent mixing in the boundary layer [see *Levy et al.*, 1982; *Kasibhatla et al.*, 1996; *Levy et al.*, 1999, and references therein].

2.1. CO, NO_x, and O_3 Simulations

[9] The GCTM simulation of CO includes sources from biomass burning (748 Tg CO/yr), fossil fuel (300 Tg CO/yr), biogenic hydrocarbon oxidation (683 Tg/yr), and CH_4 oxidation (758 Tg/yr) with OH oxidation of CO providing the only sink (see *Holloway et al.* [2000, and references therein] for details).

[10] The GCTM simulation of reactive nitrogen transports three families of tracers, NO_x, peroxyacetyl nitrate (PAN), and nitric acid (HNO_3); represents the chemical interconversions among them by effective first-order rate coefficients that have been precalculated off-line; removes HNO_3 by wet deposition and all three by dry deposition; and includes sources from fossil fuel (22.4 Tg N/yr), biomass burning (7.8 Tg N/yr), soil-biogenic emission (5 Tg N/yr), lightning (4 Tg N/yr), aircraft emissions (0.45 Tg N/yr), and stratospheric injection (0.65 Tg N/yr) (see *Levy et al.* [1999] and *Galanter et al.* [2000] for details).

[11] The GCTM simulation of tropospheric O_3 chemistry [*Yienger et al.*, 2000, 1999; *Levy et al.*, 1997; *Klonecki and Levy*, 1997; *Kasibhatla et al.*, 1996] contains the following four components. Irreversible stratospheric injection of O_3 (629 Tg O_3/yr) is driven by the GCTM's tropospheric meteorology, while its lower-stratospheric ozone values are relaxed, with a 10-day lifetime, to those simulated by the GFDL SKYHI GCM [*Hamilton et al.*, 1995; L. Perliski, private communication, 1997]. The CH_4-CO/Acetone-H_2O-NO_x based 24-hour averaged rates of ozone production and destruction in the background troposphere (NO_x <200 parts per trillion by volume (pptv) and/or isoprene <100 pptv) are interpolated each time step from precalculated FEOM (Fully Equivalent Operational Model) tables [*Wang et al.*, 1999] using the model's instantaneous O_3 levels, 6-hour sampled NO_x and CO concentrations from simulations described above, and monthly averaged observations of H_2O [*Oort*, 1983; *Soden and Bretherton*, 1996]. When NO_x exceeds 200 pptv and isoprene exceeds 100 pptv in the polluted boundary layer, ozone net production employs an empirical relationship between NO_x conversion and O_3 production based on midlatitude observations and theoretical studies [*Kasibhatla et al.*, 1996; *Levy et al.*, 1997, and references therein]. Surface dry deposition, which depends on month and vegetation [*Matthews*, 1983], is calculated using a drag-coefficient formulation for surface exchange [*Levy and Moxim*, 1989] and a standard resistance-in series model for deposition velocities [*Wesely and Hicks*, 1977; *Wesely*, 1989].

2.2. Asian Emissions

[12] The two emission regions in this study, South Asia (India, Pakistan, Bangladesh, Nepal, Sri Lanka) and Southeast Asia (Myanmar, Cambodia, Thailand, Laos, Vietnam, southeastern China) are shown in Figure 1 of *Galanter et al.* [2000] as regions 9 and 8, respectively. CO and NO_x emission intensities over South Asia are particularly high in the densely populated Gangetic plains and in southern India. Over Southeast Asia, large emissions occur over Bangkok, Singapore and southeastern China. The export of pollution to the Indian Ocean will be strongly affected by this regional distribution. For example, one of the four prominent transport paths noted during the IFP-99 of INDOEX was from the Gangetic plains of India. This in conjunction with the high emission intensities could result in large export of pollution plumes to the ITCZ.

[13] Unlike Europe and North America, where anthropogenic emissions are largely from fossil fuel combustion, in Asia emissions from biofuels and biomass burning play a key role in the regional photochemistry. A breakdown of the source categories of CO and NO_x over South and Southeast Asia is presented in Figure 1. As seen in the figure, both CO and NO_x emissions exhibit strong seasonality with an early spring peak and a late fall minimum. This seasonality is a result of emissions from biomass burning (forest fires, agricultural waste residue and savannah burning) that occurs mostly during the dry winter-spring months. Fortunately for the inhabitants, meteorology strongly correlates this biomass burning season with a winter monsoon that ventilates the region out over the Indian Ocean.

[14] Monthly mean NO_x emissions range from 0.12 TgN in late fall to ~0.2 TgN in spring over South Asia, whereas those over Southeast Asia vary between ~0.05 TgN in late fall and ~0.13 TgN in spring. During the spring biomass burning season, only ~1/2 of the South Asian and ~1/3 of Southeast Asian NO_x emissions come from fossil fuel combustion, while it dominates during summer and fall. For CO, there is a twofold increase in emissions over South Asia from ~5 Tg in summer and fall to >10 Tg in spring. Over Southeast Asia the change is even more dramatic from ~2 Tg in summer and fall to ~7 Tg in spring. Biofuel and biomass burning emissions of CO from both regions comprise a large fraction of the total CO emissions throughout the year. For example, during the winter-spring burning season, biofuels and biomass burning constitute ~90% of the total CO emissions. Inefficient combustion at low temperatures in domestic cook stoves with a biofuel feedstock results in large emissions of CO. In contrast, these low temperatures prevent the formation of thermal NO_x, leading to comparatively smaller NO_x emissions.

2.3. GCTM Meteorology Over the Indian Ocean

[15] As mentioned previously, the winter-spring mean flow over the Indian Ocean north of the ITCZ is mostly north to northeasterly in the boundary layer changing rapidly to westerly in the middle and the upper troposphere north of 20°N. In the GCTM, the monsoonal flows (both winter and summer monsoon) have been shown in the past to be adequately reproduced [*Manabe and Holloway*, 1975; *Hahn and Manabe*, 1975]. Moreover, the GCTM wind flows are generally consistent with climatological mean observations from *Oort* [1983] and a 40 year average of

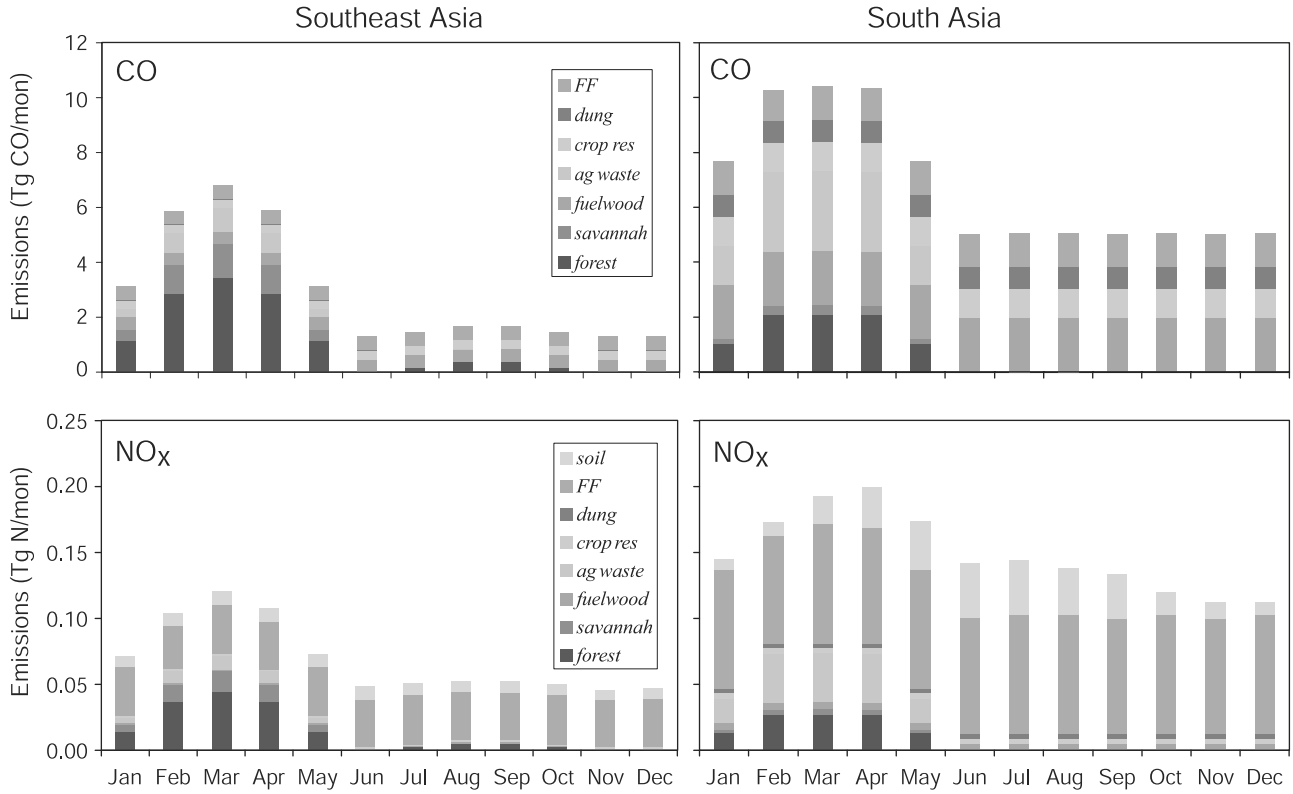

Figure 1. Monthly mean emissions of CO and NO_x over Southeast Asia and South Asia by source type (FF: fossil fuel, dung: animal waste, crop res: crop residue, ag waste: agricultural waste). See color version of this figure at back of this issue.

the NCEP winds. Here we focus our attention only on the winter monsoon.

[16] Model surface streamlines for February are shown in Figure 2. The simulated intertropical convergence zone (ITCZ) over the Indian Ocean can be clearly seen at ~5°S. Our model captures the observed [*Krishnamurti et al.*, 1998] surface inflow to the ITCZ over the Arabian sea, Bay of Bengal and Southeastern Indian Ocean. As depicted in Figure 2, surface flow over the Arabian Sea transports air masses mostly from South Asia. In contrast, surface flow over the Bay of Bengal brings air from both eastern-northeastern India, Bangladesh and Southeast Asia to the ITCZ.

[17] Since the intensive field campaign of INDOEX occurred in 1999, we compare our model's monthly mean streamlines with NCEP analysis for 1999 in Figure 2. In general the model's surface streamlines for February are consistent with the 1999 NCEP analysis, which shows similar equatorward continental outflow from both South and Southeast Asia and an ITCZ between 5°S and 10°S. The ITCZ eddy feature south of India in the NCEP 1000 mbar analysis represent a region of very weak winds. In the lower troposphere, the flow patterns and the shift from easterly to westerly flow observed in the NCEP data, as well as the northeasterly flow over Southeast Asia, are generally matched by the model, though the GCTM's westerly flow is slightly more equatorward.

[18] From the above discussion we see that the GCTM winds capture most of the observed mean flow behavior in the lower troposphere during February 1999 in the study region. Unlike the springtime outflow at midlatitudes (e.g. East Asia) where large-scale synoptic systems are responsible for long-range transport of pollutants in the middle troposphere [e.g., *Yienger et al.*, 2000], we will show that subtropical monsoonal transport of pollution is dominated by continental boundary layer outflow toward the ITCZ.

3. Model Evaluation

[19] Results from previous model simulations have been compared extensively with global data sets obtained from a variety of surface-based and upper air platforms. Model CO has been shown to compare favorably with surface measurements from the NOAA/CMDL cooperative flask sampling network (93% of seasonally averaged data points within +25%) and aircraft data from the NASA Global Tropospheric Experiment (GTE) (79% of regionally averaged data points within +25%) [*Holloway et al.*, 2000, and references therein]. The simulated NO_x fields are in reasonable agreement with observations from aircraft, primarily data from the NASA Global Tropospheric Experiment (GTE) (~50% of the regionally averaged comparisons within +25% error limits, and ~75% within +50% error limits), show no systematic global biases and exhibit the observed vertical profiles in the troposphere [*Levy et al.*, 1999, and references therein]. Ozone comparisons with over 300 seasonal observations from over 30 ozonesonde sites, 12 surface sites, and the Transport and Atmospheric Chemistry Near the Equatorial Atlantic (TRACE-A) aircraft mission find almost 90% of the simulated seasonal values in the boundary layer and

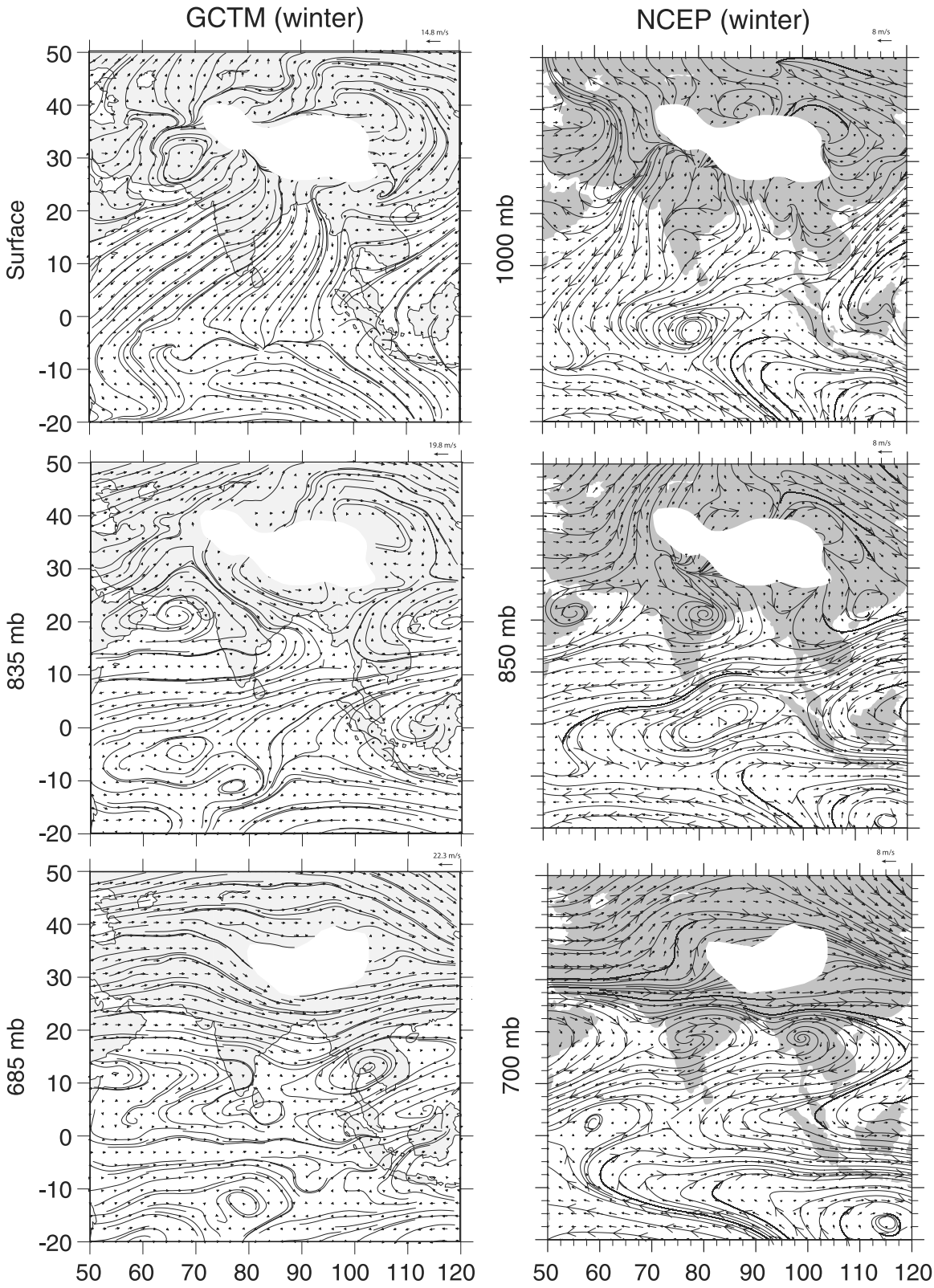

Figure 2. Monthly mean GCTM February streamlines over South Asia and tropical Indian ocean at the surface, 835 mb and 685 mb (left). Also shown are monthly mean February 1999 streamlines from NCEP reanalysis at 1000 mb, 850 mb and 700 mb (right).

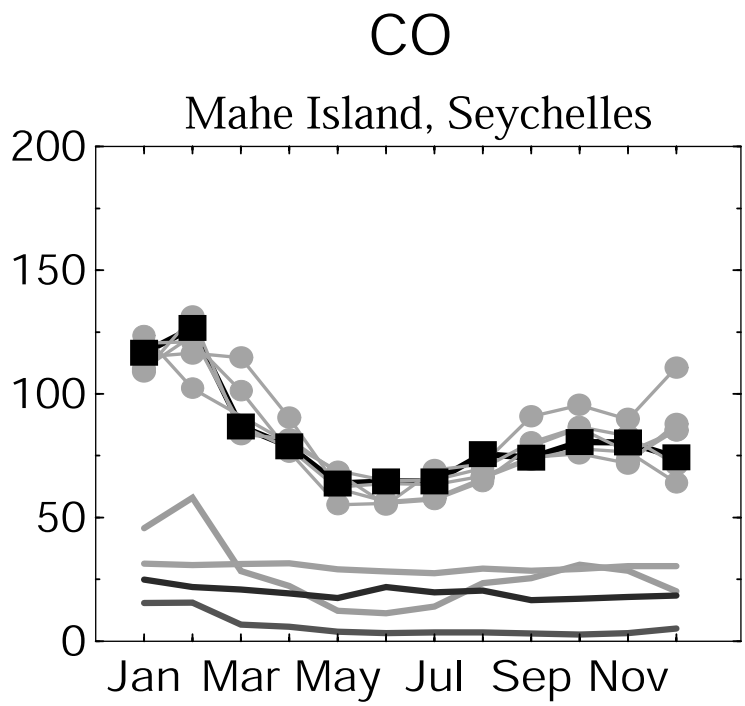

Figure 3. Time series of observed CO (purple), total simulated CO (black), as well as the simulated contribution from individual sources: fossil fuel (red), biomass burning (green), biogenic hydrocarbon oxidation (blue), methane oxidation (orange). The observations represent the years 1988–1995. See color version of this figure at back of this issue.

free troposphere agreeing to within +25% with the observations [*Yienger et al.*, 1999; *Levy et al.*, 1997].

[20] Regional evaluations over the South Atlantic [*Moxim and Levy*, 2000], North Pacific [*Yienger et al.*, 2000], and the tropical biomass burning regions [*Galanter et al.*, 2000] all found that the CO, NO_x and O_3 simulations were realistic. While there is a paucity of long-term data available for the region currently being studied (South Asia, Southeast Asia, and the Indian Ocean), we make comparisons with what is available. We also include O_3 and CO data from the INDOEX field campaign, though it should be cautioned that the INDOEX data is for a specific period, winter-spring 1999, and is not a climatology.

3.1. CO Comparisons

[21] Among reactive trace gas measurements in the region under study, those of carbon monoxide and ozone are most reliable. Because its sources and chemical sink are relatively simple, we will first focus on CO. Monthly mean mixing ratios are available for Mahe Island, Seychelles (4.7°S, 55.5°E) in the Indian Ocean from the NOAA/CMDL cooperative flask sampling network (see Figure 3, taken from *Holloway et al.* [2000]). The simulation in black, which can be seen amongst the multiple years of observations, clearly reproduces the observed magnitude and seasonal cycle at this site. Both model results and observations exhibit a winter maximum and summer minimum with a peak to peak amplitude of ~70 ppbv, which is dominated by the contribution from biomass burning (green line).

[22] Data from aircraft sampling of carbon monoxide during the INDOEX IFP-99 (http://www.joss.ucar.edu) are shown in Figure 4. We have aggregated all measurements from 11 flights within the following volume [3.5°N – 6.5°N and 72°E – 75°E] that surrounds Kaashidhoo. The boundary layer measurements exhibit particularly large variability in March with standard deviations (S.D.) of ~±100ppbv, and with the mean CO exceeding 200 ppbv. In contrast, aircraft CO measurements in February are much less variable. While there is a considerable overlap of measured and simulated S.D.'s, the observed S.D.'s are significantly larger. Comparison of the aircraft CO monthly means with model data reveals an under prediction in the lower troposphere, with model monthly means ranging between 150 and 200 ppbv in the marine boundary layer and 100–125 ppbv in the middle troposphere.

3.2. NO_x Comparisons

[23] We could not make a similar model evaluation of NO_x against observations owing to lack of a consistent good quality data for NO_x over the Indian Ocean. This can also be verified against the data composites from *Emmons et al.* [1997] and [2000]. NO_x data during the INDOEX IFP-99 and the pre-INDOEX period was too sporadic in space and time to make a detailed comparison with simulated data. In a plot of NO and NO_2 versus julian day for samples taken aboard the R/V *Malcolm Balridge*, *Rhoads et al.* [1997] show NO and NO_2 mixing ratios in the 10–20 pptv and 40–50 pptv range, respectively, on julian days when the ship was close to the Indian coast. A visual comparison with simulated NO_x in the marine boundary layer over the North Indian Ocean (Standard in Figure 9) exhibit similar values. Upper tropospheric NO_x measurements were performed on passenger aircrafts under the Swiss NOXAR project. Some of the flights in this project sampled upper tropospheric NO_x over

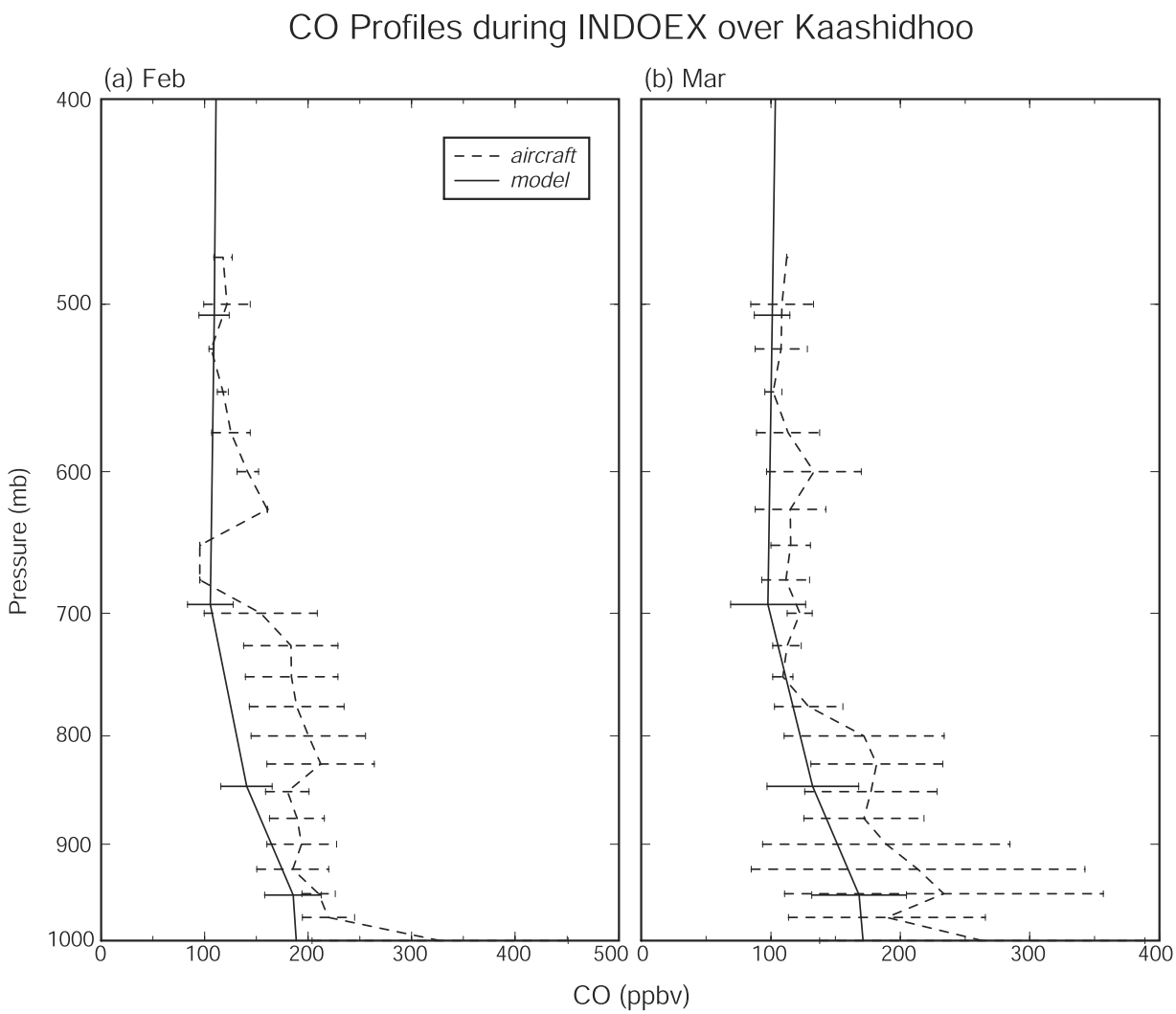

Figure 4. Mean vertical profiles of model CO for February and March and aircraft observations taken during INDOEX in the vicinity of Kaashidhoo. The aircraft data are segregated into 25 mb vertical bins.

South Asia. A comparison with simulated NO_x at 315 mb (Standard in Figure 9) with the upper tropospheric DJF and MAM NO_x samples in Plate 1 from *Brunner et al.* [2001] reveal a close agreement. Simulated NO_x is 100–200 pptv over South Asia along the flight tracks in Plate 1 of *Brunner et al.* [2001]. Measured NO_x is also in the 100–200 pptv range and increases to 200–300 pptv over Southeast Asia. A rigorous evaluation of simulated NO_x on a global scale has been performed in the past by *Levy et al.* [1999] lending credibility in the GCTM's ability to simulate global NO_x.

3.3. Ozone Comparisons

[24] In Figure 5, vertical profiles of simulated ozone JFM means and standard deviations (S.D.) are compared with observations provided by the World Ozone and Ultraviolet Data Center (WOUDC), Environment Canada, Downsview, Ontario (http://www.msc-smc.ec.gc.ca/woudc) for Delhi, India (29°N, 77°E), Pune, India (19°N, 74°E), and Trivandrum, India (9°N, 77°E). The observed JFM means and S.D.'s are for 1994 – 1999 and are calculated from 16, 13, and 24 ozonesondes respectively. While the model captures the observed vertical profiles of ozone with simulated and observed S.D.'s overlapping, a general bias exists with observed means exceeding simulated means by 10–25ppbv at Delhi and Pune. Furthermore, the observed S.D.'s exceed those simulated throughout the middle and upper troposphere.

[25] Also shown in Figure 5 are the vertical profiles of simulated and observed ozone for Hong Kong (22°N, 114°E). The ozone data (57 ozonesondes) was obtained from S. J. Oltmans (personal communication) for the period 1994–2000. Except for a modest positive model bias in the boundary layer and upper troposphere, simulated and observed O_3 exhibit excellent agreement throughout the troposphere. Compared with the Indian ozonesondes, there is much less variability in both simulated and measured O_3.

[26] Ozonesondes were launched regularly over Kaashidhoo (5°N, 73.5°E) in Maldives off the southern tip of India during the INDOEX IFP-99. The results are provided by the SHADOZ website (http://hyperion.gsfc.nasa.gov/Data_services/shadoz/Kaashidhoo.html [*Thompson et al.*, 2002]) for January, February and March with 5, 26 and 22 ozonesondes, respectively. Vertical profiles of monthly mean observed and simulated ozone with their S.D.'s are

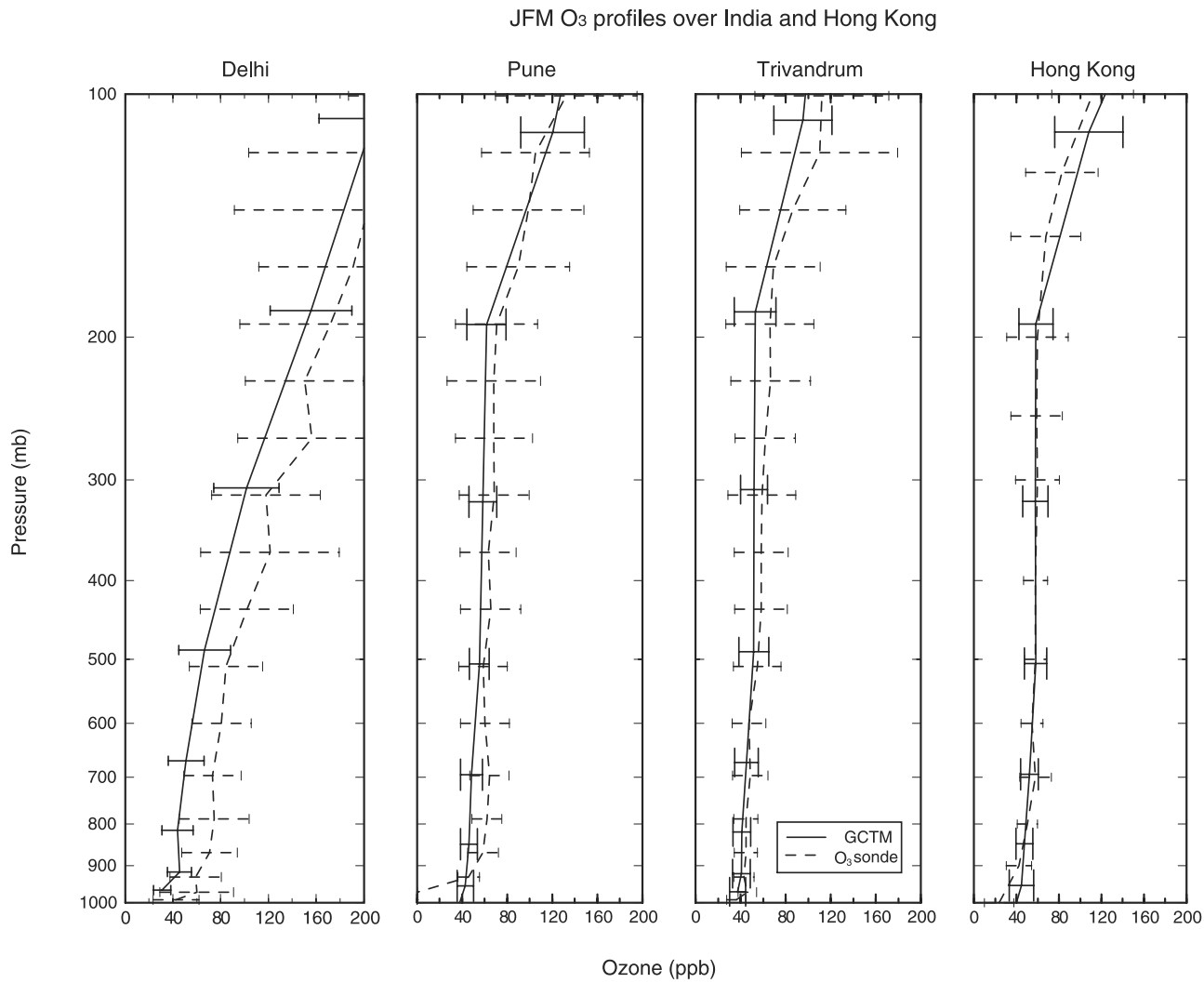

Figure 5. Vertical profiles of mean winter (JFM) O_3 over Delhi, Pune and Trivandrum, India as well as Hong Kong, China from model calculations (solid lines) and ozonesonde measurements (dashed lines).

presented in Figure 6. The February overlap is very good, while the January and March simulated profiles show overestimations of 10–20 ppbv above 500 mb, in contrast with the overestimations in Figure 5. These overestimations at Kaashidhoo may be attributed to the O_3 sonde measurements carried out very frequently only during spring 1999 and thus reflecting effects of time-specific emissions and meteorology. In contrast, the O_3 sonde measurements in Figure 5 were for several years and thus minimize any bias from an individual time period. The other major disagreements are found in the lower troposphere. The GCTM produces a maximum in the boundary layer, which is not generally observed in February and March, and does not simulate the observed March O_3 maximum at 800 mb. This maximum was also observed for some pollutants during the aircraft sampling of INDOEX IFP-99, particularly in March. It was attributed to a "residual pollution layer" originating from the Indian continental boundary layer [*Reiner et al.*, 2001], a high resolution feature that the GCTM is unable to simulate. On the other hand, the March aircraft sampling of CO found at most a slight bump at 800 mb with the CO maximum in the marine boundary layer as simulated by the GCTM.

[27] Aircraft sampling of ozone was also carried out during February and March 1999 in the vicinity of Kaashidhoo and their monthly means and S.D.'s are presented in Figure 6 as the dashed lines. The February GCTM and ozonesonde O_3 agree more closely with each other than either agrees with the aircraft observations. Above 700 mb, the O_3 mixing ratios measured from aircraft in February drop to <10 ppbv, while both the model O_3 and the ozonesonde observations remain in the 40 ppbv range. In March neither the GCTM nor aircraft mean O_3 profiles show an 800 mb maximum, though some individual flights do exhibit a local maximum at ~800 mbar with values exceeding 45 ppbv. The vertical profiles of O_3 from aircraft measurements in the vicinity of Kaashidhoo exhibit considerable variability from one flight to another and have little in common with the Kaashidhoo ozonesondes. The large differences in the aircraft O_3 and model O_3 can be attributed to the fact tha the aircraft data was averaged over a number of flights on different days crossing the model grid box over Kaashidhoo. We believe the low O_3 sampled by the aircraft must be originating from a clean mass of air. One would have to conduct actual back trajectory analyses on the sampled aircraft data to understand the origin of the clean

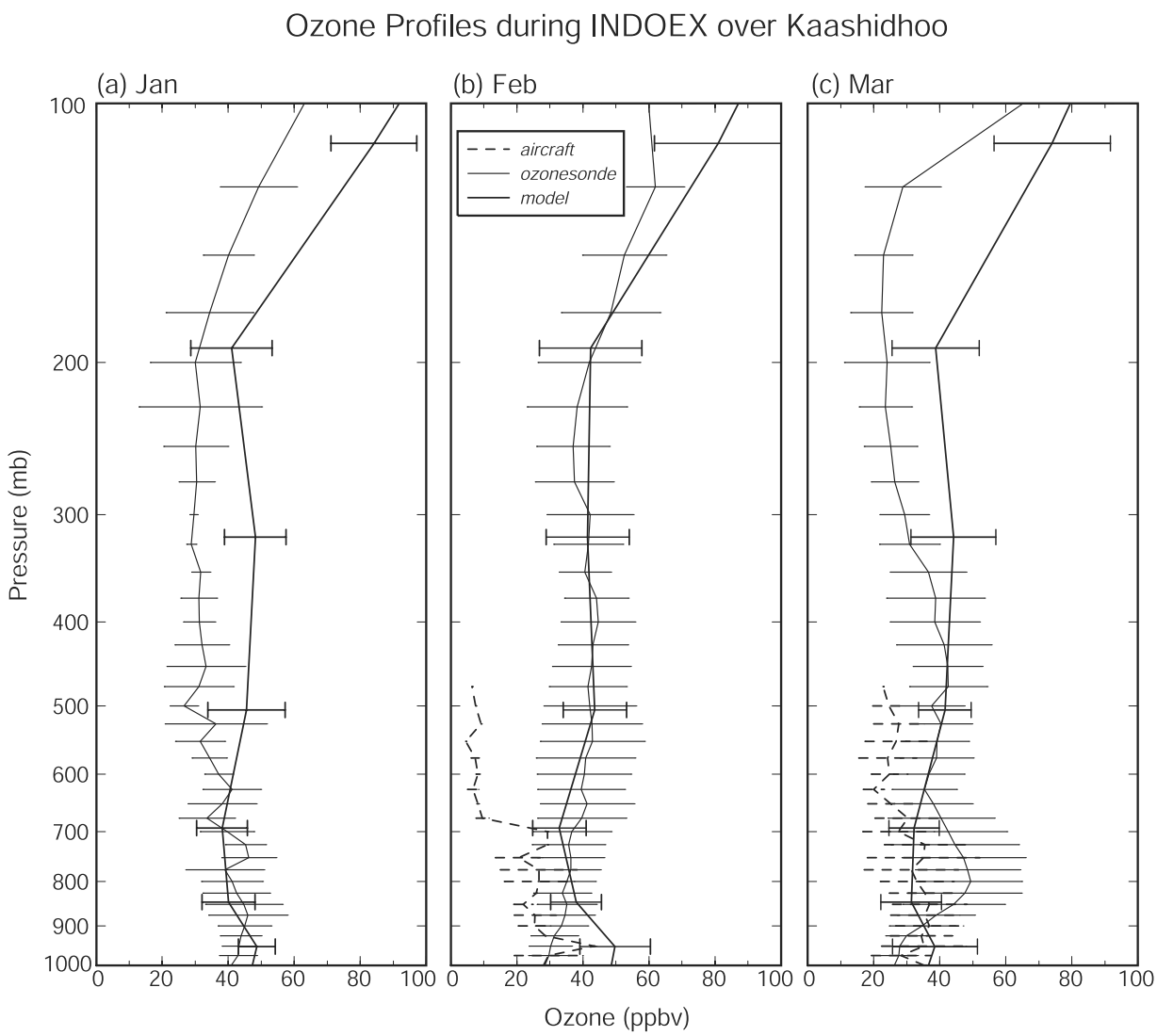

Figure 6. Vertical profiles of February and March monthly mean O_3 and their standard deviations over Kaashidhoo from model calculations (thick solid line) and ozonesonde measurements (thin solid line). Note that the ozonesonde measurements are for 1999 only. Also shown are the monthly mean vertical O_3 profiles from aircraft data (dashed lines). The aircraft data are segregated into 25 mb vertical bins.

versus polluted air. This analyses is beyond the scope of the current work since in this manuscript we are examining climatological features.

[28] In general the GFDL GCTM captures the basic features in the ozonesondes over India and over Kaashidhoo, though the aircraft observations of O_3 do not particularly agree with either model or ozonesonde. It was generally concluded from the IFP-99 that the JFM ozone levels over India were unusually low, by as much as 15–20% from the 1998 values, in agreement with the general quasi-bienniel variation [*Mitra et al.*, 2000]. This may explain part of the apparent bias between the model and surface observation, as well as between climatological and IFP-99 observations.

4. Model Simulations

[29] From the previous discussion, we see that the GCTM simulations capture most of the features observed in measurements over South Asia and the neighboring Indian Ocean, with the major exceptions being the March 800 mb O_3 bulge and the elevated boundary layer CO, both at Kaashidhoo. We argue that the model simulations of O_3, and CO are realistic enough to explore in detail the large-scale features of their distributions over the region and to examine the geo-political source regions that influence the tropospheric composition over the Indian Ocean during the winter monsoon.

[30] Specifically, we present analyses which separately examine the impact of emissions from South Asia and Southeast Asia on air quality over the Indian Ocean. Emissions were turned off separately and those simulations then subtracted from a base case with all anthropogenic sources to produce the contributions from the two source regions to total CO, NO_x and O_3 levels. The same base-state linear chemistry is used for all NO_x and CO simulations to avoid unintentional and inappropriate chemical feedbacks and to provide an unambiguous answer.

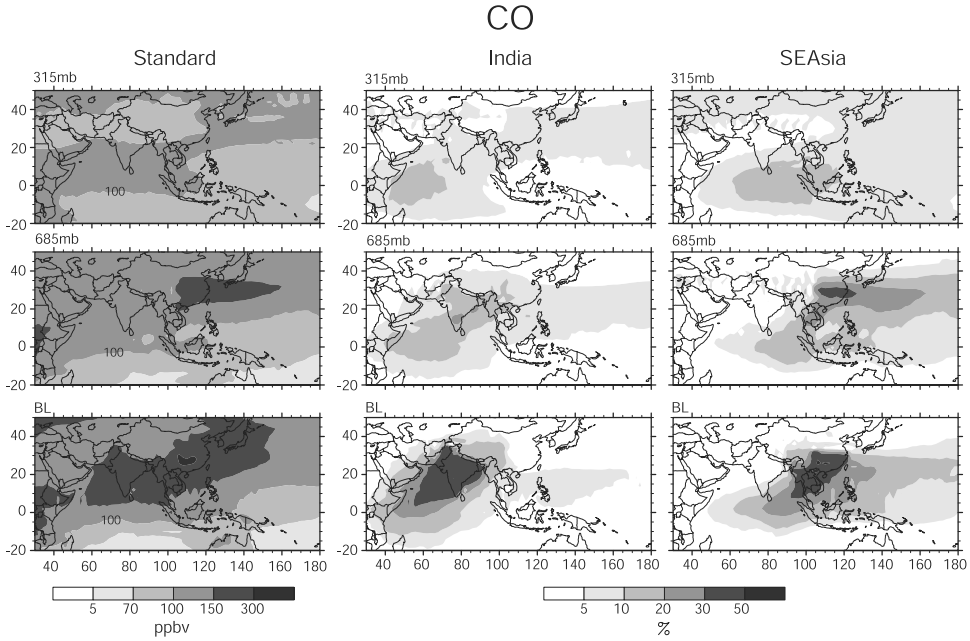

Figure 7. Mixing ratios of total CO (left) during January, February and March (JFM). Contributions from South Asian (middle) and Southeast Asian (right) fossil fuel and biomass burning are given as a percent of the total CO. BL - boundary layer mixing ratios are calculated as weighted average of the three lowermost model layers (990 mb, 940 mb and 850 mb).

[31] The identification of the two source region's contribution to the total O_3 level is more complex. It is not possible to unambiguously identify those O_3 molecules produced by a particular regions emissions, as we can for NO_x and CO. O_3 chemistry depends nonlinearly on NO_x and CO levels [see *Klonecki and Levy*, 1997, Figures 1 and 10], O_3 formation can be a product of precursors and radicals from different regions, and it is not possible to maintain the same chemistry for O_3 simulations with differing CO and NO_x emissions. What we can present is the change in O_3 when a particular region's emissions are shut down.

4.1. Regional CO Distributions

[32] We first focus on CO, which, with its relatively long chemical lifetime of a month or more [e.g., *Holloway et al.*, 2000], is an excellent tracer for identifying the key transport paths and processes that apply to all trace species in the region. Large-scale features of the simulated mean JFM CO levels over the region of interest are presented in Figure 7 for 315 mb, 685 mb and the boundary layer (mass weighted average of the lowest three model levels). The first column (Standard) presents the total CO, the 2nd column (SAsia) is for % CO from surface pollution of South Asia, and the 3rd column (SEAsia) is for % CO from surface pollution of Southeast Asia.

[33] Simulated boundary layer total CO over South and Southeast Asia and the northern Indian Ocean generally exceeds 150 ppbv (simulated levels are >300 ppbv over Southeast China). Because of widespread biomass burning over Southeast which peaks in March, simulated total CO mixing ratios increase from January to March and are in the 400–600 ppbv range in March. A clear transition between the polluted and pristine boundary layers is evident between the equator and 10°S, the location of the Indian Ocean ITCZ during this time of the year, with total CO mixing ratios south of the ITCZ dropping to 50–70 ppbv. This boundary layer picture is consistent with observations from INDOEX [*Lelieveld et al.*, 2001]. In the lower troposphere at 685 mbar, total CO levels over most of the NH portion of the region are 100–150 ppbv and display the general background gradient. East Asia is an exception with the lifting of surface pollution by synoptic-scale systems as well as local convection producing higher levels (150–250 ppbv). In the upper troposphere [315 mb] the most distinctive feature is a maximum total CO stretching from the ITCZ to 20°N that is explained below.

[34] Also shown in Figure 7 are the individual % contributions to total CO from South and Southeast Asian CO emissions, which, as discussed previously in Figure 1, are dominated by biomass burning. In the boundary layer, South Asian CO contributes 30–50% of the total CO over the source region, the Arabian Sea, and the western Bay of Bengal with the fraction increasing to 80% in the 990 mb level. Southeast Asian CO emissions make a similar contribution over their source region and contribute 20–30% over the western tropical Pacific and the eastern Bay of Bengal. Over the western Bay of Bengal, most observed CO is emitted from the Gangetic plains of India and transported via the "Gangetic Plume" as discussed in INDOEX [*Lelieveld et al.*, 2001]. While the GCTM can not resolve this high resolution detail, it does capture the continental outflow over the Bay of Bengal. Moving south over the Indian Ocean, the contributions from South and Southeast Asian generally drop to 10–20% at the ITCZ. It is interesting to note that, while each pollution region has a separate area of maximum impact over the Indian Ocean, the sum of their impacts is relatively constant across the equatorial Indian

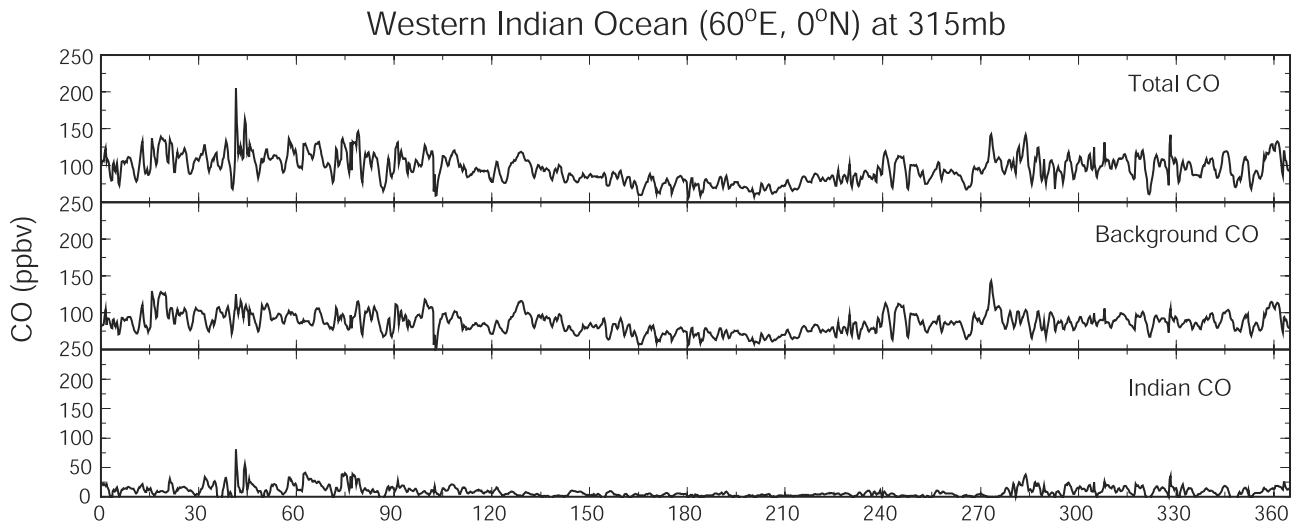

Figure 8. Time series of total CO, background CO and South Asian CO over the Western (60°E, 0°N) Indian Ocean at 315 mb. Background CO is the difference between the total CO and South Asian CO.

Ocean. Our model results agree closely to the modeled surface and upper tropospheric biomass burning CO from India and Southeast Asia from the work of *de Laat et al.* [2001]. A detailed discussion of the contributions from other CO sources is provided by *Holloway et al.* [2000].

[35] A distinct lowering of the influence of surface emissions is seen as we move up in the troposphere. At 685 mbar, the CO attributed to the South and Southeast Asian sources constitute ~30% of the total CO over the source regions as well as 10–20% over the western and eastern portions of the Indian Ocean, respectively. The one exception is over southern China and the eastern Pacific where Southeast Asian CO contributes more than 30%. This flow of CO from biomass burning in Southeast Asia is consistent with an earlier analysis of springtime air quality observations in Hong Kong [*Chan et al.*, 2000].

[36] In the upper troposphere (315 mb), there is a maximum influence (10–20%) from both source regions over the tropical Indian Ocean. In association with the low-level continental outflow, CO from South and Southeast Asia is carried southward in the marine B.L. to the ITCZ, where, due to its low solubility in cloud water, it is efficiently transported aloft by strong local convection. The pollution CO is then carried north and south in the upper tropospheric outflow while slowly spreading westward in the upper level easterlies. These local maxima of South and Southeast Asian CO, which are clearly disconnected from the source regions, produce the 315 maximum noted earlier.

[37] To examine the 315 mb total CO maximum in more detail, we focus in Figure 8 on a local equatorial CO time series at 60°E which is located in a region of maximum South Asian impact. Total 315 mb CO, which is plotted at the top, exhibits a winter-spring maxima with increased variability and a number of large spikes, particularly around Julian day 45. The middle time series shows the background 315 mb CO, which excludes pollution CO from South Asia. It also has a winter-spring maxima, but has much reduced variability. The bottom time series is for the same location at 315 mb, but includes only pollution CO from South Asia. It has a number of high frequency spikes of a very high relative amplitude, again with a winter-spring maximum. While similar winter-spring events of pollutant CO have already been simulated in the mid and upper troposphere at midlatitudes over the North Pacific [*Yienger et al.*, 2000], they arose from synoptic-scale systems which are absent in the tropics. We believe that the large South Asian CO spikes in Figure 8 identify an important seasonal transport path from South Asia to the tropical upper troposphere. The winter-spring monsoon produces a maximum in continental outflow of seasonal pollutants, while intermittent convective transport drives the high variability seen in the tropical 315 mb time series.

[38] While the primary focus of this paper is the Indian Ocean region, there is another transport path that features Southeast Asian emissions. Lower tropospheric flow (see 835 mb streamlines in Figure 2) carries emissions from Southeast Asia northeastward, along with southern China emissions, into eastern China where both are then transported in a midlatitude plume over the eastern North Pacific. This Southeast Asian CO plume then continues in the middle troposphere across the North Pacific, North America and out over the North Atlantic (not shown in Figure 7). This transport path was previously discussed in a simulation paper by *Yienger et al.* [2000] as well as in an observation and analysis paper by *Chan et al.* [2000].

4.2. Regional Distributions of NO_x

[39] The winter-spring (JFM) NO_x fields in Figure 9 retain many of the transport derived patterns displayed by CO in Figure 7. However, in the lower troposphere the gradients are stronger, as are the continental source impacts over the Indian Ocean. This is due to a much shorter chemical lifetime for NO_x (~1 day) and a lack of significant sources over the Indian Ocean [*Levy et al.*, 1999]. The total B.L. NO_x field decreases from >500 pptv over the continental source regions to 20 pptv at the equator, while the N-S gradient at 685mb for total NO_x (100pptv to <20 pptv) is somewhat weaker. There is no tropical maximum at

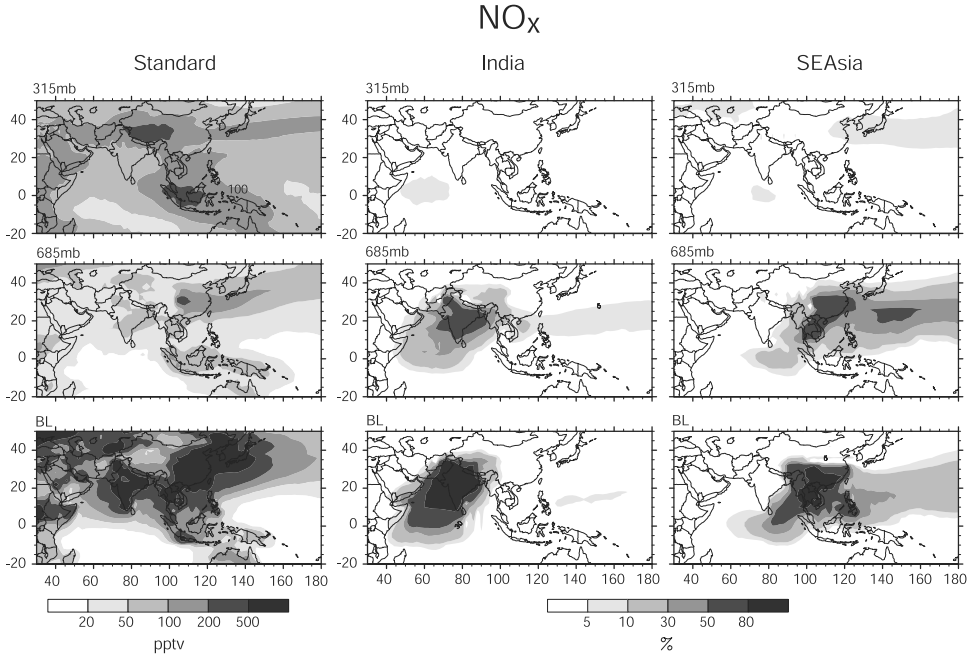

Figure 9. Same as Figure 7, except for NO_x.

315 mb as there was for CO. A relatively high NO_x (>100 pptv) at 315 mb over Indonesia is seen in Figure 7. Referring to Plate 1 of *Levy et al.* [1999], during DJF at 315 mb, the dominant source of NO_x over Indonesia is lightning. Moreover, ~25% of surface NO_x emissions are also convected in the upper troposphere over Indonesia [see *Levy et al.*, 1999, Figure 9]. In our modeling, we assume Indonesia to be tropical Asia and hence it has not been included in Southeast Asia.

[40] The relative impacts of South and Southeast Asian NO_x are significantly larger than they were for CO in the northern Indian Ocean, though not as widespread. Over half of the NO_x in the B.L. and 10–30% at 685 mb over the Indian Ocean north of the equator were emitted in South and Southeast Asia and transported equatorward in the low level continental outflow discussed previously. Just as for CO, there is also a strong lower tropospheric transport of Southeast Asian NO_x to eastern China and out over the eastern North Pacific. In the upper troposphere, however, the contribution from surface NO_x emissions is much smaller and more confined than it was for CO. While both species are insoluble in water, the relatively long transport times required to reach convective regions such as the ITCZ and the short chemical life time of NO_x results in little continental NO_x being available for convective transport, though there is still a small signature at 315 mb. The dominance of long range transport from the South and Southeast Asian source regions by low level flow in the warm MBL precludes a significant role for the indirect transport of NO_x by PAN.

4.3. Regional Distributions of O_3

[41] The forces controlling O_3 are much more complex than are those determining the distributions of CO and NO_x. All three species experience the same two primary transport mechanisms discussed earlier: 1. Low level continental outflow over the Indian Ocean to the ITCZ followed by convective lifting; 2. Northeastward transport from Southeastern Asia to southern China and the western Pacific with both convective and large-scale lifting into the lower and mid troposphere. However, besides direct production in the polluted continental B.L., O_3 has a chemical source in the background troposphere, which is strongly modulated by transported NO_x, and a strong episodic injection of O_3 from the stratosphere.

[42] The overall horizontal patterns in the lower troposphere for the winter-spring (JFM) total O_3 fields shown in Figure 10 generally fall between those found for NO_x and CO. This reflects a common N-S gradient in B.L. emissions for all three species and O_3's intermediate lower tropospheric lifetime (~1 week). In the B.L., total O_3 levels south of the ITCZ are <20 ppbv increasing to >40 ppbv north of 5°N. However, unlike CO and NO_x, O_3 mixing ratios increase with height throughout the troposphere while maintaining an equator to pole gradient. In the tropical upper troposphere there is an O_3 minimum where, unlike CO, the normal latitudinal O_3 gradient is reinforced by convective transport of lower O_3 mixing ratios from the tropical MBL.

[43] The impact of South and Southeast Asian emissions on O_3 is dominated by NO_x emissions which have comparable contributions from both fossil fuel combustion and biomass and biofuel burning. There are two major roles played by these emissions: 1. The production of O_3 (later called pollution O_3) in the emission region followed by its export; 2. The export of NO_x by low level continental outflow over the Indian Ocean to change the net chemical tendency for O_3 in that region from destruction to production. For Southeast Asian emissions there is also transport over eastern China and out over the eastern Pacific. As can be seen in Figure 9, the winter-spring NO_x levels are maintained at >100 pptv all the way to 5°N in the B.L.

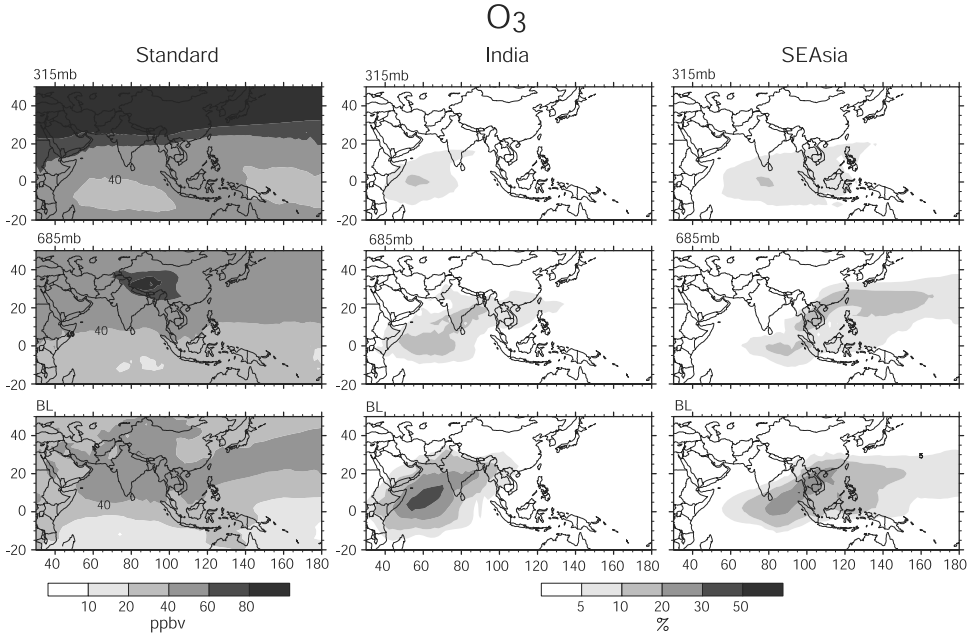

Figure 10. Same as Figure 7, except for O_3.

over the Indian Ocean and over eastern China and the North Pacific in the B.L. and the lower troposphere.

[44] Interestingly, the maximum contributions to B.L. ozone from both source regions, particularly from South Asia with a >30% contribution, are out over the tropical Indian Ocean, rather than simply spreading from the continental source regions. The localized B.L. maxima result from the lower tropospheric transport mechanisms for both source regions, consisting of subsidence over the source region with low level outflow into the Indian Ocean B.L. to the ITCZ. The outflow from South Asia carries O_3 produced in the source regions into the marine B.L. along with NO_x that maintains net O_3 production down to ~5°N. Over the source regions the impact of pollution, though not the actual concentration of O_3, is diluted by elevated background O_3 from the free troposphere transported in down-slope flow from the north (Himalayan plateau region). As a result, the maximum contribution from South and Southeast Asian emissions occurs out over the Indian Ocean, not over the source regions.

[45] While the patterns are unchanged, South and Southeast Asian contributions to O_3 decrease with altitude. Although there is a minimum for total O_3, local maxima in O_3 from South and Southeast Asian emissions are seen in the 315 mb panel of Figure 10 in the same locations found for CO. This is consistent with our hypothesis that strong convection lifts transported surface pollution into the upper troposphere over the equatorial Indian Ocean.

[46] Further detail is provided by a simulation that separately labels the O_3 produced in the polluted continental boundary layer. While it is impossible to directly identify and quantify an individual contribution with available observational data, we can do so with our GCTM (see *Moxim and Levy* [2000] for numerical details). The mean JFM distributions of O_3 chemically produced in the polluted South and Southeast Asian continental boundary layer are shown in Figure 11. Note that this is only one component of the total impact of South and Southeast Asian emissions on tropospheric O_3. We first consider the boundary layer. Even over the polluted continent, less than 25% of the total O_3 results from local chemical production, which implies a large fraction being supplied from the free troposphere. Further note that, at the equator, O_3 chemically produced in the polluted continental boundary layer only accounts for ~15% of the total, while Figure 10 shows surface emissions from South and Southeast Asia suppling ~30% of the total. This is consistent with the surface emissions both producing O_3 locally and supplying precursors for O_3 production in the continental outflow. At 315 mb, pollution O_3 exhibits a tropical maximum and supplies ~10% of the total 315 mb O_3 in the same location where South and Southeast Asian emissions have already been shown (see Figure 10) to be responsible for a similar percentage. This is consistent with convective lifting of the pollution O_3 and with the fact that 315 mb O_3 chemistry is not significantly affected by the small amount of pollution NO_x lifted to that level (see Figure 9). This behavior of pollution O_3 is a further consistency check of the transport mechanism we have proposed.

[47] Again, as seen for CO and NO_x, the impacts of South Asian pollution on O_3 are primarily confined to the Indian Ocean region, while the impact of Southeast Asian pollution, albeit somewhat weaker over the Indian Ocean, stretches in a midlatitude lower tropospheric plume (5–10%) across the North Pacific. Unlike CO, the O_3 plume does not reach across North America and the North Atlantic, since both it and its primary precursor, NO_x, have much shorter lifetimes.

5. Conclusions and Summary

[48] In this study, we employed the GFDL GCTM to examine the role of South and Southeast Asian anthropogenic emissions in the continental outflow of pollution to the Indian Ocean during the winter-spring transition (Jan-

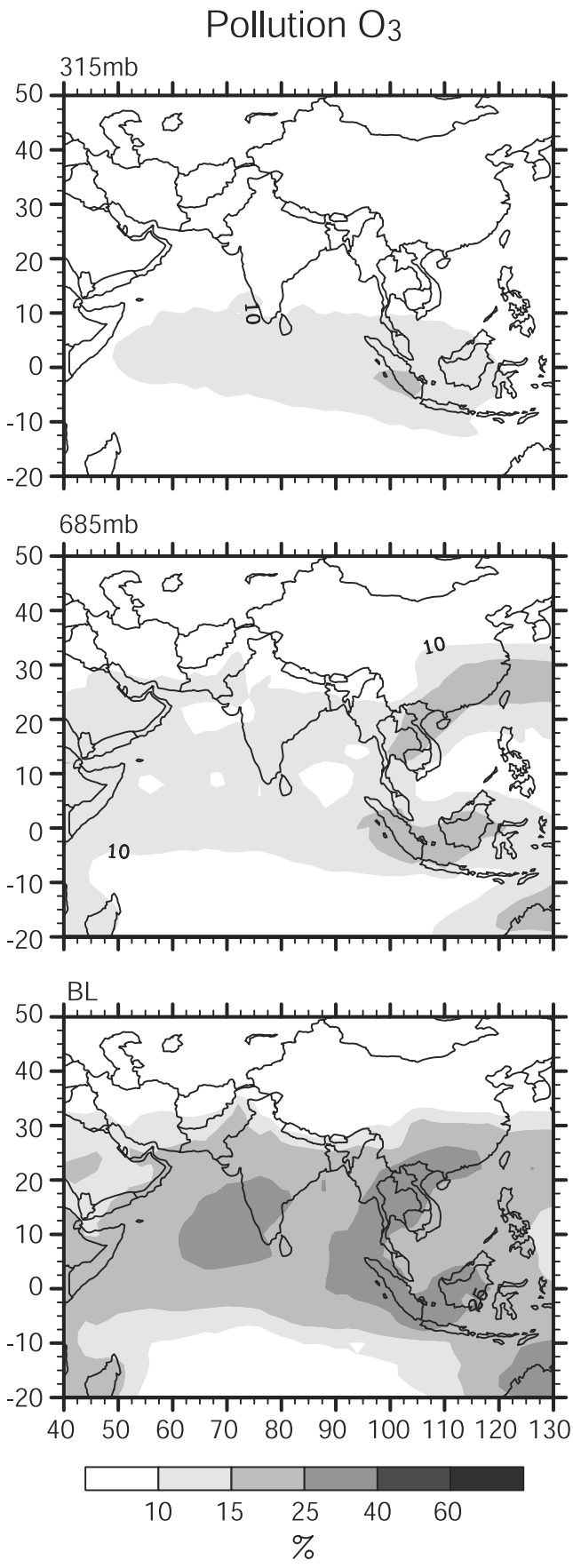

Figure 11. The percent contribution of O_3 produced in the polluted boundary layer [Pollution O_3] to the total O_3.

uary, February and March), a period of maximum surface emissions from both South and Southeast Asia. During this period, surface emissions of CO are mostly from biomass burning activities over the two regions, while surface NO_x emissions arise almost equally from biomass burning and fossil fuel combustion. The model's agreement with the Seychelles CO surface climatology was excellent, while agreement with aircraft measurements of CO from INDOEX in 1999 was favorable in the middle troposphere with a low model bias in the boundary layer. Model simulations of the vertical O_3 structure over South and Southeast Asia was generally realistic with both GCTM and sonde O_3 mixing ratios increased from 40–50 ppb in the boundary layer to >100 ppb at the tropopause. Over Kaashidhoo, GCTM O_3 profiles and O_3 sonde data from INDOEX exhibited a good overlap in February. However, the model over predicted the O_3 sonde observations in the middle and upper troposphere in January and March. Aircraft measurements of O_3 in the vicinity of Kaashidhoo during March and February did not agree with either the GCTM simulations or the ozonesonde observations.

[49] Our analysis on the evolution of pollution from the South and Southeast Asia can be summed up in the following paragraphs.

1. Simulated CO at the surface over the Indian Ocean is in the 50–300 ppb range with high values closer to land and the lowest mixing ratios over the equatorial Indian Ocean. The combined contributions of South and Southeast Asian surface emissions to surface CO levels range from 20–50%. CO over the Arabian Sea originates mainly from South Asia, while over the Bay of Bengal CO comes from Southeast Asia.

2. In the upper troposphere, both South and Southeast Asian CO contribute 10–20% to a local maximum over the equatorial Indian Ocean. This is the result of low-level continental outflow coupled to strong convection around the ITCZ and represents an important seasonal transport path from South Asia to the tropical upper troposphere.

3. Because of the very short lifetime of NO_x, surface NO_x exhibits a very strong gradient (<20 pptv to >500 pptv) from the equator to sub-tropical Asia and also a strong decrease of South and Southeast Asian NO_x from the surface to the upper troposphere.

4. South and Southeast Asian emissions exhibit a maximum contribution to boundary layer O_3 (>30%) over the ocean rather than over source regions, with both direct transport of pollution O_3 and O_3 produced from transported precursors contributing. Both O_3 and NO_x contributions from South and Southeast Asia exhibit an equatorial maximum in the upper troposphere as did CO, lending credibility to the proposed upper tropospheric transport path driven by continental outflow coupled to tropical convection.

5. While the impacts of anthropogenic emissions from South Asia during winter-spring is mostly restricted to the Indian Ocean region, Southeast Asian emissions have influence over both the Indian Ocean and the North Pacific Ocean. This implies a greater spatial influence for Southeast Asian emissions on global air quality, photochemistry and radiation balance.

[50] Since both South and Southeast Asian emissions are projected to grow significantly in the future, long term measurements are needed over the Indian Ocean, Arabian

Sea and the Bay of Bengal to better constrain regional and global atmospheric chemistry and transport models. Intensive TRACE-P type measurements campaigns during the winter- spring outflow season over the Indian Ocean are needed to quantify the export of pollutants to the tropical troposphere and across the ITCZ.

[51] **Acknowledgments.** We would like to thank Larry W. Horowitz for his comments in preparation of this manuscript. The measurement data were taken from the INDOEX website at NCAR. M.J.P would like to thank the Princeton Environmental Institute for support though the Cleveland Dodge fellowship.

References

Benkovitz, C. M., M. T. Sholtz, J. Pacyna, L. Tarrason, J. Dignon, E. C. Voldner, P. A. Spiro, J. A. Logan, and T. E. Graedel, Global gridded inventories of anthropogenic emissions of sulfur and nitrogen, *J. Geophys. Res.*, *101*, 29,239–29,253, 1996.

Brunner, D., J. Staehelin, D. Jeker, H. Wernli, and U. Schumann, Nitrogen oxides and ozone in the tropopause region of the Northern Hemisphere: Measurements from commercial aircraft in 1995/1996 and 1997, *J. Geophys. Res.*, *106*, 27,673–27,699, 2001.

Chan, L. Y., C. Y. Chan, H. Y. Liu, S. Christopher, S. J. Oltmans, and J. M. Harris, A case study on the biomass burning in Southeast Asia and enhancements of tropospheric ozone over Hong Kong, *Geophys. Res. Lett.*, *27*, 1479–1482, 2000.

de Laat, A. T. J., J. Lelieveld, G. J. Roelofs, R. R. Dickerson, and J. M. Lobert, Source analysis of carbon monoxide pollution during INDOEX 1999, *J. Geophys. Res.*, *106*, 28,481–28,495, 2001.

Emmons, L. K., et al., Climatologies of NO_x and NO_y: A comparison of data and models, *Atmos. Environ.*, *31*, 1851–1904, 1997.

Emmons, L. K., D. A. Hauglustaine, J.-F. Muller, M. A. Carroll, G. P. Brasseur, D. Brunner, J. Staehelin, V. Thouret, and A. Marenco, Data composites of airborne observations of tropospheric ozone and its precursors, *J. Geophys. Res.*, *105*, 20,497–20,538, 2000.

Galanter, M., H. Levy II, and G. R. Carmichael, Impacts of biomass burning on tropospheric CO, NO_x, and O3, *J. Geophys. Res.*, *105*, 6633–6653, 2000.

Hahn, D. G., and S. Manabe, The role of mountains in the S. Asian monsoon circulation, *J. Atmos. Sci.*, *32*, 1515–1541, 1975.

Hamilton, K. P., R. J. Wilson, J. D. Mahlman, and L. Umscheid, Climatology of the SKYHI troposphere-stratosphere-mesosphere general circulation model, *J. Atmos. Sci.*, *52*, 5–43, 1995.

Holloway, T. A., H. Levy II, and P. S. Kasibhatla, Global distribution of carbon monoxide, *J. Geophys. Res.*, *105*, 12,123–12,147, 2000.

Intergovernmental Panel on Climate Change (IPCC), *Third Assessment Report: Climate Change 2001*, edited by R. T. Watson and the Core Writing Team, Cambridge Univ. Press, New York, 2001.

Johnson, J. E., R. H. Gammon, J. Larsen, T. S. Bates, S. J. Oltmans, and J. C. Farmer, Ozone in the marine boundary layer over the Pacific and Indian Oceans: Latitudinal gradients and diurnal cycles, *J. Geophys. Res.*, *95*, 11,847–11,856, 1990.

Kasibhatla, P., H. Levy II, A. A. Klonecki, and W. L. Chameides, Three-dimensional view of the large-scale tropospheric ozone distribution over the North Atlantic Ocean during summer, *J. Geophys. Res.*, *101*, 29,305–29,316, 1996.

Klonecki, A. A., and H. Levy II, Tropospheric chemical ozone tendencies in $CO\text{-}CH_4\text{-}NO_y\text{-}H_2O$ system: Their sensitivity to variations in environmental parameters and their application to a global chemical transport model study, *J. Geophys. Res.*, *102*, 21,221–21,237, 1997.

Krishnamurti, T. N., B. Jha, P. J. Rasch, and V. Ramanathan, A high resolution global reanalysis highlighting the winter monsoon, part I, Reanalysis fields, *Meteorol. Atmos. Phys.*, *64*, 123–150, 1997a.

Krishnamurti, T. N., B. Jha, P. J. Rasch, and V. Ramanathan, A high resolution global reanalysis highlighting the winter monsoon, part II, Transients and passive tracer transports, *Meteorol. Atmos. Phys.*, *64*, 151–171, 1997b.

Krishnamurti, T. N., B. Jha, J. Prospero, A. Jayaraman, and V. amanathan, Aerosol and pollutant transport and their impact on radiative forcing over the tropical Indian Ocean during the January–February 1996 pre-INDOEX cruise, *Tellus, Ser. B*, *50*, 521–542, 1998.

Lal, S., M. Naja, and A. Jayaraman, Ozone in the marine boundary layer over the tropical Indian Ocean, *J. Geophys. Res.*, *103*, 18,907–18,917, 1998.

Lelieveld, J., et al., The Indian Ocean Experiment: Widespread air pollution from South and Southeast Asia, *Science*, *291*, 1031–1036, 2001.

Levy, H., II, and W. J. Moxim, Simulated global distribution and deposition of reactive nitrogen emitted by fossil fuel combustion, *Tellus*, *41*, 256–271, 1989.

Levy, H., II, J. D. Mahlman, and W. J. Moxim, Tropospheric N_2O variability, *J. Geophys. Res.*, *87*, 3061–3080, 1982.

Levy, H., II, J. D. Mahlman, W. J. Moxim, and S. C. Liu, Tropospheric ozone: The role of transport, *J. Geophys. Res.*, *90*, 3753–3772, 1985.

Levy, H., II, P. S. Kasibhatla, W. J. Moxim, A. A. Klonecki, A. I. Hirsch, S. J. Oltmans, and W. L. Chameides, The global impact of human activity on tropospheric ozone, *Geophys. Res. Lett.*, *24*, 791–794, 1997.

Levy, H., II, W. J. Moxim, A. A. Klonecki, and P. S. Kasibhatla, Simulated tropospheric NO_x: Its evaluation, global distribution, and individual source contributions, *J. Geophys. Res.*, *104*, 26,279–26,306, 1999.

Logan, J. A., et al., Trends in the vertical distributions of ozone: A comparison of two analyses of ozone data, *J. Geophys. Res.*, *104*, 26,373–26,399, 1999.

Mahlman, J. D., and W. J. Moxim, Tracer simulations using a global general circulation model: Results from a midlatitude instantaneous source experiment, *J. Atmos. Sci.*, *35*, 1340–1374, 1978.

Manabe, S., and J. L. Holloway Jr., The seasonal variation of the hydrologic cycle as simulated by a global model of the atmosphere, *J. Geophys. Res.*, *80*, 1617–1649, 1975.

Manabe, S., D. G. Hahn, and J. L. Holloway Jr., The seasonal variation of the tropical circulation as simulated by a global model of the atmosphere, *J. Atmos. Sci.*, *31*, 43–83, 1974.

Matthews, E., Global vegetation and land use: New high-resolution data bases for climate studies, *J. Clim. Appl. Meteorol.*, *22*, 474–487, 1983.

Mitra, A. P., A. Jayaraman, B. V. Krishnamurthy, U. C. Mohanty, and G. Viswanathan, INDOEX-India Program Synthesis Report, Palampur, India, 2000.

Moxim, W. J., Simulated transport of NO_y to Hawaii during August: A synoptic study, *J. Geophys. Res.*, *95*, 5717–5729, 1990.

Moxim, W. J., and H. Levy II, A model analysis of the tropical South Atlantic Ocean tropospheric ozone maximum: The interaction of transport and chemistry, *J. Geophys. Res.*, *105*, 17,393–17,415, 2000.

Moxim, W. J., H. Levy II, and P. S. Kasibhatla, Simulated global tropospheric PAN: Its transport and impact on NO_x, *J. Geophys. Res.*, *101*, 12,621–12,638, 1996.

Naja, M., and S. Lal, Changes in surface ozone amount and its diurnal and seasonal patterns, from 1954–55 to 1991–93, measured at Ahmedabad (23 N), India, *Geophys. Res. Lett.*, *23*, 81–84, 1996.

Olivier, J. G. J., et al., Description of EDGAR Version 2.0: A set of global emission inventories of greenhouse gases and ozone-depleting substances for all anthropogenic and most natural sources on a per country basis and on $1^\circ \times 1^\circ$ grid, 141 pp., *RIVM Rep. 771060*, Natl. Inst. of Public Health and the Environ., Bilthoven, Netherlands, 1996.

Oort, A. H., Global atmospheric circulation statistics, 1958–1973, *NOAA Prof. Pap. 14*, 180 pp., Natl. Oceanic and Atmos. Admin., Washington, D. C., 1983.

Ramanathan, V., et al., Indian Ocean Experiment (INDOEX) (C^4 publication 162), Univ. of Calif., San Diego, 1996. (Available at http://www.c4-ucsd.edu)

Rhoads, K. P., P. Kelley, R. R. Dickerson, T. P. Carsey, M. Farmer, D. L. Savoie, and J. M. Prospero, Composition of the troposphere over the Indian Ocean during the monsoonal transition, *J. Geophys. Res.*, *102*, 18,981–18,995, 1997.

Reiner, T., D. Sprung, C. Jost, R. Gabriel, O. L. Mayol-Bracero, M. O. Andreae, T. L. Campos, and R. E. Shetter, Chemical characterization of pollution layers over the tropical Indian Ocean: Signatures of emissions from biomass and fossil fuel burning, *J. Geophys. Res.*, *106*, 28,497–28,510, 2001.

Soden, B. J., and F. P. Bretherton, Interpretation of TOVS water vapor radiances in terms of layer-average relative humidities: Method and climatology for the upper, middle, and lower troposphere, *J. Geophys. Res.*, *101*, 9333–9343, 1996.

Streets, D. G., and S. T. Waldhoff, Biofuel use in Asia and acidifying emissions, *Energy*, *23*, 1029–1042, 1998.

Thompson, A. M., et al., The 1998–2000 SHADOZ (Southern Hemisphere Additional Ozonesondes) tropical ozone climatology: Comparisons with TOMS and ground-based measurements, *J. Geophys. Res.*, *107*, doi:10.1029/2001JD000967, in press, 2002.

van Aardenne, J. A., G. R. Carmichael, H. Levy II, D. Streets, and L. Hordijk, Anthropogenic NO_x emissions in Asia in the period 1990–2020, *Atmos. Environ.*, *33*, 633–646, 1999.

Wang, S. W., H. Levy II, G. Li, and H. Rabitz, Fully equivalent operational models for atmospheric chemical kinetics within global chemistry-transport models, *J. Geophys. Res.*, *104*, 30,417–30,426, 1999.

Wesely, M. L., Parameterization of surface resistances to gaseous dry deposition in regional-scale numerical models, *Atmos. Environ.*, *23*, 1293–1304, 1989.

Wesely, M. L., and B. B. Hicks, Some factors that affect deposition rates of sulfur dioxide and similar gases on vegetation, *J. Air Pollut. Control Assoc.*, *27*, 1110–1116, 1977.

Yienger, J., A. A. Klonecki, H. Levy II, W. J. Moxim, and G. R. Carmichael, An evaluation of chemistry's role in the winter-spring ozone maximum found in the northern midlatitude free troposphere, *J. Geophys. Res.*, *104*, 3655–3667, 1999.

Yienger, J. J., M. Galanter, T. A. Holloway, M. J. Phadnis, S. K. Guttikunda, G. R. Carmichael, W. J. Moxim, and H. Levy II, The episodic nature of air pollution transport from Asia to North America, *J. Geophys. Res.*, *105*, 26,931–26,945, 2000.

H. Levy II and W. J. Moxim, Geophysical Fluid Dynamics Laboratory, NOAA, Princeton, NJ 08542, USA. (hl@gfdl.gov)

M. J. Phadnis, Earth Tech, Inc., 196 Baker Avenue, Concord, MA 01742-2167, USA.

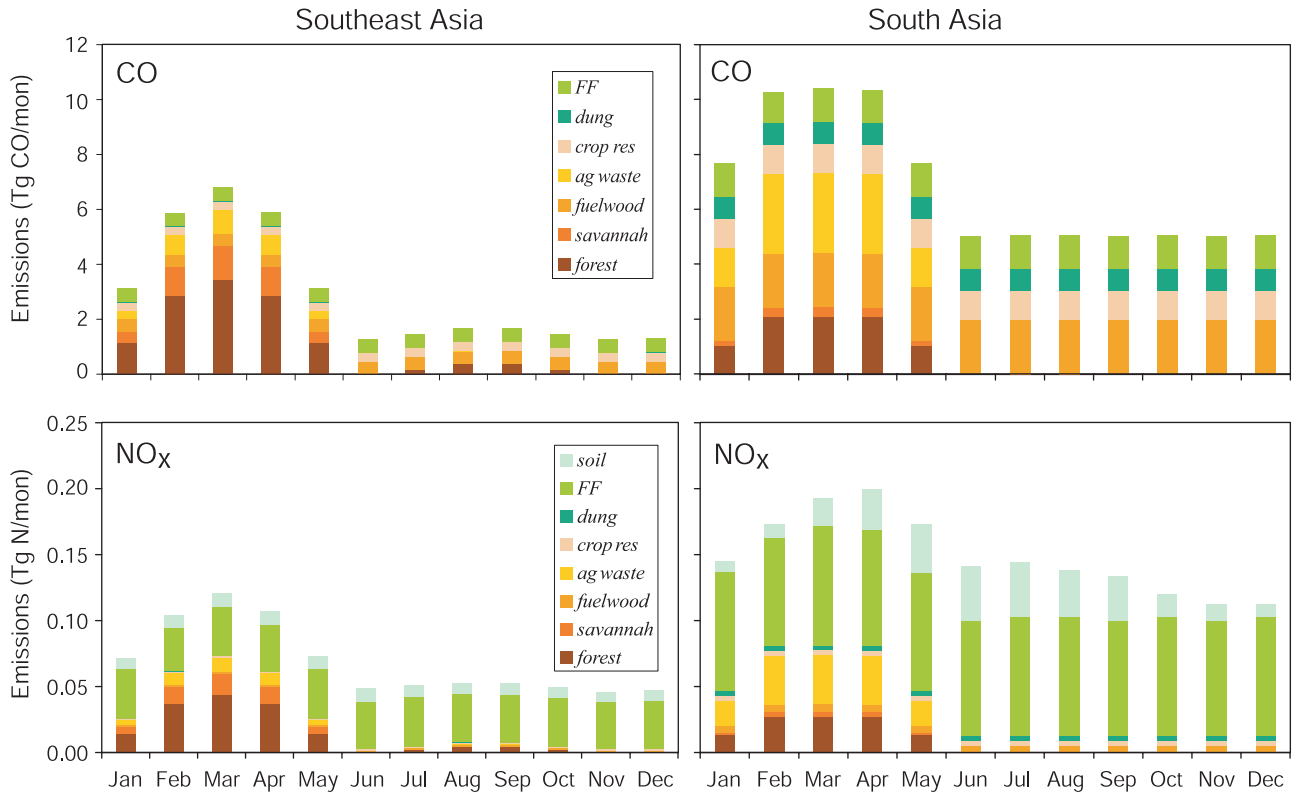

Figure 1. Monthly mean emissions of CO and NO_x over Southeast Asia and South Asia by source type (FF: fossil fuel, dung: animal waste, crop res: crop residue, ag waste: agricultural waste).

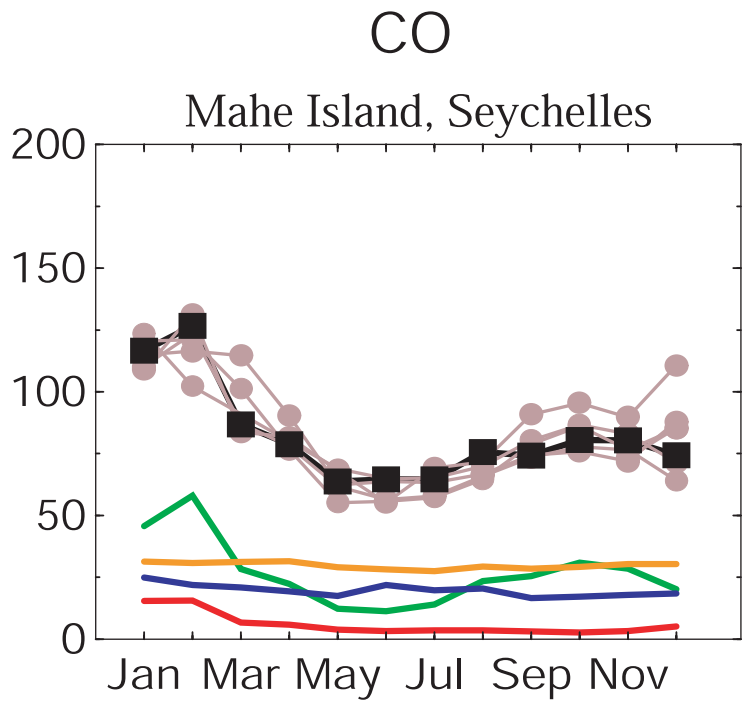

Figure 3. Time series of observed CO (purple), total simulated CO (black), as well as the simulated contribution from individual sources: fossil fuel (red), biomass burning (green), biogenic hydrocarbon oxidation (blue), methane oxidation (orange). The observations represent the years 1988–1995.